Anal. Bioanal. Electrochem., Vol. 13, No. 2, 2021, 160-175

Analytical&
Bioanalytical
Electrochemistry

Full Paper

Investigation on Tin Electrodeposition from Sulphuric Acid Medium

S. Bakkali,[1,2] M. Cherkaoui,[2] I. Warad,[3] and A. Zarrouk[4,*]

[1]*Laboratoire de Chimie Analytique et Moléculaire/LCAM, Université Cadi Ayyad, Faculté Polydisciplinaire, Sidi Bouzid, B.P. 4162, 46 000 Safi, Morocco*
[2]*Laboratoire de Matériaux d'Electrochimie et d'Environnement, Faculté des Sciences, Université Ibn Tofaïl,14000Kénitra, Morocco*
[3]*Department of Chemistry and Earth Sciences, P.O. Box 2713, Qatar University, Doha, Qatar*
[4]*Laboratory of Materials, Nanotechnology and Environment, Faculty of Sciences, Mohammed V University in Rabat, P.O. Box. 1014, Rabat, Morocco*

*Corresponding Author, Tel.: +212 665 201 397. Fax.: +212 537 774 261
E-Mail: azarrouk@gmail.com

Received: 7 July 2020 / Received in revised form: 13 August 2020 / Accepted: 23 August 2020 / Published online: 30 September 2021

Abstract- The tin electrodeposition in an acidic sulphate solution is reported. Electrochemical techniques (chronoamperometry, cyclic and linear voltammetry) are used to find out some kinetic parameters that govern the tin electrodeposition process while scanning electron microscopy (SEM) is used to explore the morphology of the coating. The influence on the tin electrodeposition of certain experimental parameters such as tin ion concentration, potential scan rate and deposition current density are described. Sharifker–Hills and Palomar Pardavé models are used to investigate the nucleation process of tin. It is found that the tin and proton reductions occur simultaneously. Dimensionless current-time transient related only to the tin reduction reaction fits well the theoretical transient for instantaneous mechanism nucleation. The diffusion coefficient has been determined by various electrochemical techniques and is found to be between 6.24×10^{-6} and 7.4×10^{-6} cm^2s^{-1}. i_0 the exchange current density value is 0.0023 A/cm^2 and the charge transfer coefficient α_c is approximately 0.5. It is also noted that the deposition current density affects the morphology of the deposited tin.

Keywords- Tin electrodeposition; Sulphuric acid; Voltammetry; Chronoamperometry; SEM

1. INTRODUCTION

Nowadays, pure tin electroplating has become the most popular surface coating process for lead-free components because of the regulatory restrictions, which impose limitations on the use of lead-containing materials. Tin is non-toxic and readily available. It has good soldering properties and high corrosion resistance [1,2]. These desirable properties make the application of tin suitable in a wide range of fields such as the electronic, electrotechnical, and food processing industries [3-7]. More recently, the electrodes containing tin electroplated, used as anodes in lithium-ion batteries, have yielded promising results [8-11].

In general, the tin deposit is obtained from acidic stannous sulphate or methane sulfonic acid (MSA) based electrolytes [12,13]. MSA has had a lot of success in the last decade because it has low corrosivity and a low oxidation rate to stannic ions [14,15].

Recently, growing interest has been given to the electrodeposition from the acid sulphate solution in particular for the future generation of electronic components [16-19]. Without organic additives, the tin film obtained from acidic electrolytes is dendritic. Despite the considerable number of studies about tin electrodeposition, little attention has been paid to study the solutions without additives because most research has focused on suppressing dendrite formation by adding organic additives to the plating solutions. Recently, dendritic tin electrodeposited has shown encouraging results as electrodes for electrochemical reduction of carbon dioxide [20-23].

The aim of the present study is to investigate the electrodeposition tin from an acidic sulphate solution and find out the effects of some experimental parameters on the tin electrodeposition reaction and on the morphology of the deposit. To accomplish this study, voltammetric, chronoamperometric and SEM techniques are used.

2. EXPERIMENTAL

The electrochemical experiments are carried out in a conventional, three-electrode cell. The reference electrode is a saturated calomel electrode (SCE). Pt wire is the counter electrode. The working electrode is a copper disk with a surface area of 0.28 cm^2. The electronic system used throughout the experiments consisted of a VoltaLab potentiostat/galvanostat, Model PGZ 100, interfaced with a microcomputer, running voltamaster 4 Software. Analytical grade reagents are used in the studied solutions. All experiments are performed at room temperature (25 °C). The pH of the solutions is 2. The SEM observations are made with a scanning electron microscope LEO 1530 FEG kind.

3. RESULTS AND DISCUSSION

3.1. cyclic voltammetry study

Figure 1 shows the cyclic voltammogram recorded in solution containing 0.14 M $SnSO_4$ and 0.56 M H_2SO_4 on copper electrode at 10 mV/s from -350 mV to -600 mV/SCE. As can be

noted, in the direct scan no electrochemical activity is observed before -460mV/SCE. Then a single cathodic peak is observed at around -494 mV/SCE. This peak corresponds to the reduction of Sn^{2+} into Sn metal that occurs in a single two-electron step [24-26] as described in equation 1:

$$Sn^{2+} + 2e^- \rightarrow Sn \quad (1)$$

As potentials become more negative, a plateau current appears indicating that the reduction of Sn^{2+} is controlled by the diffusion of tin ions. A further rise in the potential toward the cathodic side leads to an increase in the cathodic current because of the hydrogen evolution, which is associated with stannous ion reduction. The cathodic current recorded during the reverse sweep is higher than for the forward scan. This could be associated with the increase of the active surface area due to the formation of dendritic deposit according to the results that will be presented below. In addition, an anodic peak is observed at around -385 mV, confirming the single two-electron oxidation step to stannous ion of the tin formed during the cathodic scan according to equation 2 [24].

$$Sn \rightarrow Sn^{2+} + 2e^- \quad (2)$$

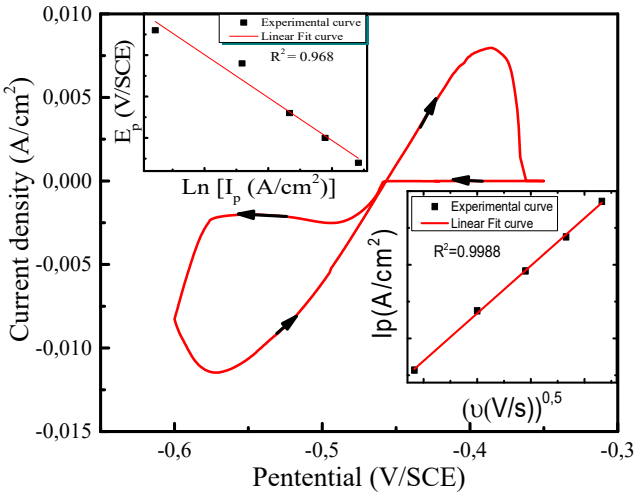

Fig. 1. Cyclic voltammogram of Sn deposition on Cu electrode at a scan rate of 10 mV s^{-1} in solution containing 0.14 M of $SnSO_4$ and 0.56 M of H_2SO_4. Cathodic peak current densities I_{pc} vs. the *square root* of the *scan rates* $\sqrt{\upsilon}$ *and* cathodic *peak potential vs. Ln(* I_{pc}) are plotted in the insets

This could be associated with the increase of the active surface area due to the formation of dendritic deposit

To examine whether the charge transfer in the system under study corresponds to a reversible or irreversible reaction, the diagnostic criteria for a reversible process predicted by cyclic voltammetry theory are used at 25 °C (Eq. 3 and Eq. 4) [27,28]:

$$\left|E_{pc} - E_{pc/2}\right| = \frac{56.5}{n} = 28.25 \text{ (mV)} \quad (3)$$

$$\left|E_{pc} - E_{pa}\right| = \frac{59}{n} = 29.5 \text{ (mV)} \quad (4)$$

Where, E_{pc} and E_{pa} are the cathodic and the anodic peak potential respectively, $E_{pc/2}$ the half cathodic potential and n = 2 is the number of electrons involved in the rate-determining step.

Table 1 presents some parameters relative to the voltammograms recorded at different scan rates. The table shows clearly that the obtained values significantly exceed the quantities characteristic of a reversible process. Furthermore, Sn^{2+}/Sn does not fulfil the diagnostic tests for a quasi-reversible system, which state that I_{pc} and I_{pa} are equal [29] and that I_{pc} is not proportional to $\sqrt{\upsilon}$ [27]. In fact the inset graph in Figure 1 shows a good proportionality between I_{pc} and $\sqrt{\upsilon}$.

Equations 5 and 6 [27,28,31] may be used as diagnostic criteria for irreversible reaction.

$$E_p = E^{0\prime} - \frac{RT}{n\alpha_c F} Ln\left(4.4\frac{nFSC_0}{k^0}\right) - \frac{RT}{n\alpha_c F} Ln(I_p) \quad (5)$$

$$\left|E_{pc} - E_{pc/2}\right| = \frac{48}{n\alpha_c} \quad (6)$$

In these equations $E^{0\prime}$ is the formal potential, α_c is the cathodic charge transfer coefficient, F is the Faraday constant, C_0 is the bulk concentration of Sn^{2+}, k^0 is the heterogeneous electron transfer rate constant, S is the electrode surface and R is the gas constant.

The inset graph in Figure 1 exhibits a linear relationship between E_p and $Ln(I_p)$ as expected by equation 5 for an irreversible system. Hence, Sn^{2+}/Sn is an irreversible system in our experimental conditions. Such behaviour was mentioned in the reference in slightly different condition [24,30,31]. From the slope of the curve, we found α = 0.5.

Table 1. Some parameters of cyclic voltammograms at different potential scans

Scan rate (mV/s)	E_{pc} (mV_{SCE})	$E_{pc/2}$ (mV_{SCE})	I_{pc} (mA/cm^2)	E_{pa} (mV_{SCE})	I_{pa} (mA/cm^2)	$I_{pa/Ipc}$	E_{pc}-E_{pa} (mV_{SCE})	$E_{pc/2}$-E_{pc} (mV_{SCE})	α_c
20	-497	-450	12.85	-382	38.73	3.01	-115	46	0.51
40	-501	-452	16.87	-373	44.33	2.63	-128	49	0.49
60	-507	-461	19.58	-366	46.13	2.36	-141	46	0.52
80	-510	-464	21.89	-364	49.74	2.27	-146	46	0.52
100	-513	-466	24.30	-358	51.64	2.13	-155	47	0.51

Table 1 gives the values of α_c obtained from equation 6 at different scan rate. As it can be seen, α_c is found to be approximately 0.51±0.01. The obtained α_c values are quit and are in line with the value mentioned in the bibliography [32].

3.2. Potentiodynamic measurements

Figure 2 shows the potentiodynamic curve recorded for tin deposition at a copper disk electrode at 2 mV S^{-1}. The rate of Sn(II) reduction may be quantitatively described by the kinetic equation 7 [33]:

$$i = i_0 \left[\exp\left(\frac{\alpha_a nF}{RT}\eta\right) - \frac{[Sn^{2+}]_s}{[Sn^{2+}]_b} \exp\left(-\frac{\alpha_c nF}{RT}\eta\right) \right] \quad (7)$$

$$\text{with} \quad \frac{[Sn^{2+}]_s}{[Sn^{2+}]_b} = 1 - \frac{i}{i_{lim}} \quad (8)$$

where $[Sn^{2+}]_b$ and $[Sn^{2+}]_s$ are respectively the bulk and the surface concentration of Sn^{2+}. i_{lim} is the current limit density, i_0 the *exchange current* density, η is the overpotential and α_a is the anodic charge transfer coefficient.

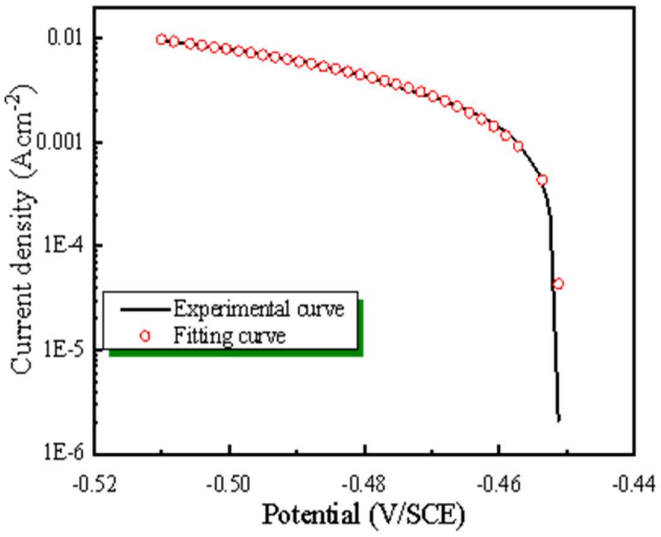

Fig. 2. Comparison of experimental and fitting data using a non-linear fitting with equation 7 obtained from the electrolyte Composed of 0.14 M $SnSO_4$ and 0.56 M H_2SO_4. at ν=2 mV s^{-1} for copper electrode

To evaluate the parameters i_0, and α_c the nonlinear curve fitting from origin Pro 9.1 was used to fit the experimental voltammogram to equation 7. We found i_0 = 0.0023 A/cm^2 and α_c=0.5. The α_c value is similar to that found above.

3.3. Effect of Sn^{2+} concentration

Figure 3 gives the voltammograms obtained at different concentrations of stannous ions. This figure shows that the current density increases with increasing the concentration of the electroactive space. Furthermore, the potential range, within which the cathodic current remains constant, decreases as the concentration of Sn^{2+} increases.

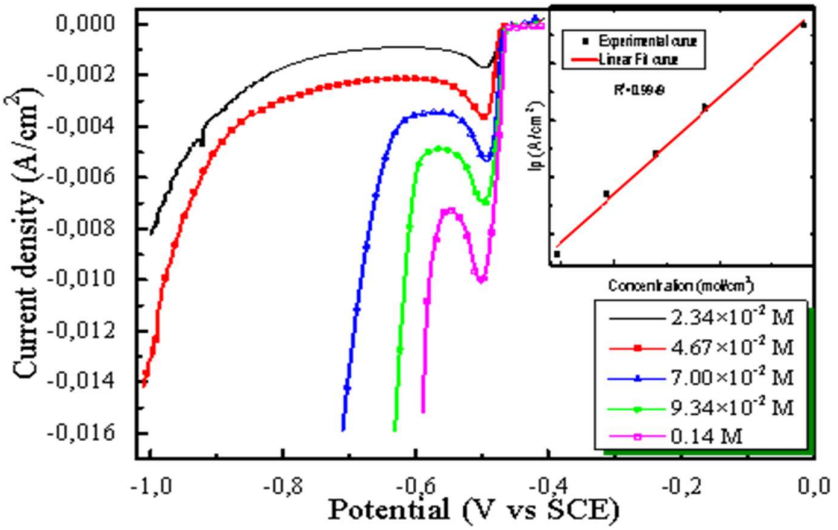

Fig. 3. Linear voltammogram of Sn deposition on Cu electrode in solution containing 0.56 M of H_2SO_4 and different concentrations of tin ion. Peak current densities (j_p) vs

tin ion concentrations are plotted in the inset

Indeed, at a low concentration, a uniform film formed of a high number of small nuclei is electrodeposited [34] during the scan of the potential. Therefore, the area of the electrode active surface remains constant. On the other hand, the rise in the current density observed in high concentration solutions is related to the fact that when the concentration increases, the deposit becomes dendritic. As a result, the real active surface of the electrode increases substantially. The reduction peak current for an irreversible system is given by equation 9 [27,28,31]:

$$I_p = -2.99x10^5 n(\alpha_c n)^{0.5} S D^{0.5} \nu^{0.5} C \qquad (9)$$

where D and ν represent diffusion coefficient and scan rate.

The *inset* graph in Figure 3 shows the curve that connects the peak current density I_p to the concentration of tin ion C. I_p and C are deduced from Figure 3. The graph exhibits good linearity ($R^2 = 0.9949$) between I_p and C according to the equation 9. The D value is estimated from the slope of the curve. D is found to be approximate 6.5×10^{-6} cm^2s^{-1}.

3.4. Surface morphology

The morphology of tin films electrodeposited at -10 and -30 mA/cm^2 from solution containing 0.14 M Sn^{2+} and 0.56 M H_2SO_4 at 2000 tr/mn was studied by SEM. Figure 4 displays the effect of the current density on the morphology of the deposit. At low current density (-10 mA/cm^2), the deposit shows the formation of a dendritic deposit (Fig. 4a). While at a high current density, (-30 mA/cm^2) dendritic and *porous* film is electrodeposited (Fig. 4b). The porosity of the deposit is due to the hydrogen evolution. In fact, porous deposits are the consequence of the incorporation in the crystal lattice of hydrogen bubbles due to the formation of the H_2 at higher current densities. As can be seen, the dendritic aspect of the coating provides an additional active surface for the electrochemical reactions. These findings are in good agreement with the results obtained by the voltammetry studies shown in Figure 3.

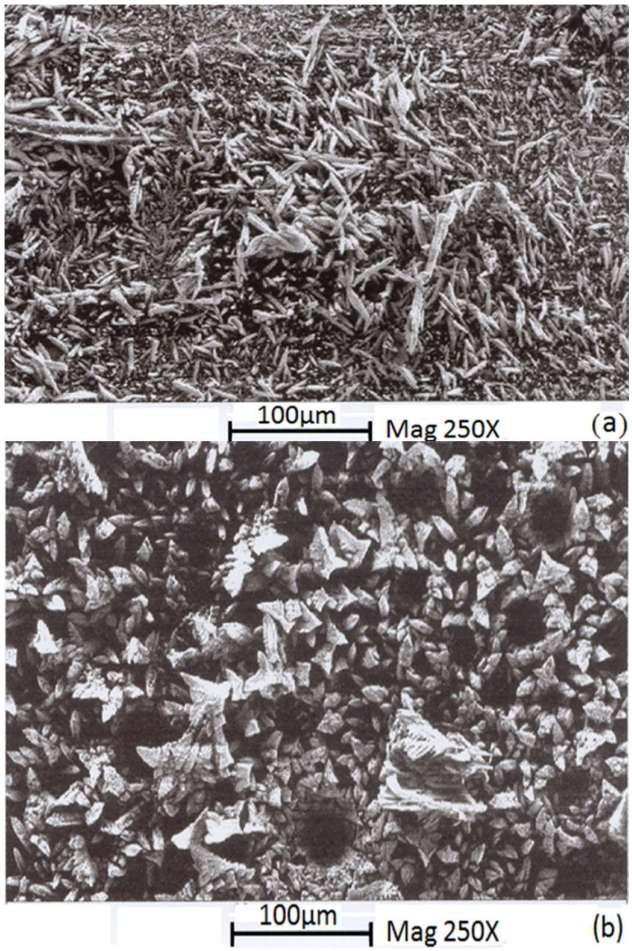

Fig. 4. Morphology of tin electrodeposited on copper electrode from 0.14 M $SnSO_4$ + 0.56 M H $_2SO_4$ at Ω = 2000 rpm (a): I = − 10 mA cm^{-2} and (b): I = − 30 mA cm^{-2}

3.5. Chronoamperometry and nucleation modeling

In order to study the nucleation mechanism in the early stages of Sn electrodeposition, chronoamperometric experiments are carried out in solution containing 0.14 M Sn^{2+} and 0.56 M H_2SO_4. The transient currents are obtained by stepping the cathode potential from the open-circuit potential to different potentials (-500, -540 or -580 mV/SCE).

During a short duration, the current-time transient curves (Fig. 5) show an increase in current caused by the nucleation and growth of tin particles. After reaching the maximum, the current decreases because of the diffusion of the tin ions from the bulk solution towards the electrode surface. Such a feature characterizes a three-dimensional nucleation and growth process occurring under the diffusion control.

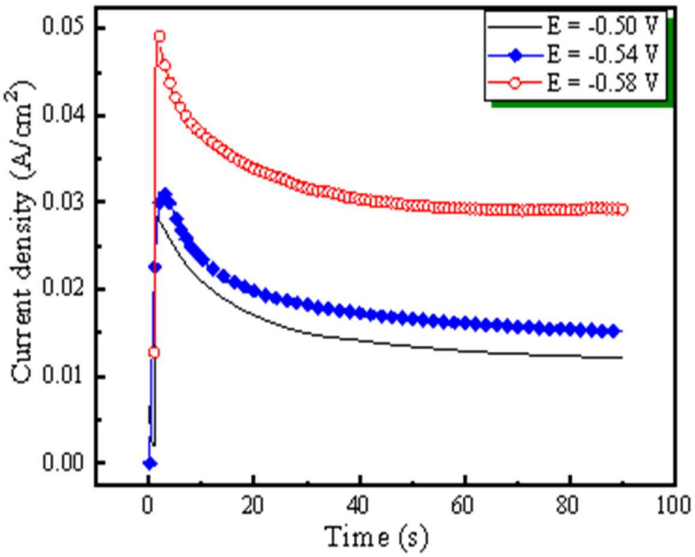

Fig. 5. Chronoamperometric curves for tin deposition on copper electrode at different potentials in solution containing 0.14 M of $SnSO_4$ and 0.56 M of H_2SO_4

Figure 6 presents i versus $t^{-1/2}$ plots at different potentials. The linear dependence of i on $t^{-1/2}$, observed in Figure 6 denotes that the tin electroreduction is controlled by diffusion. While the presence of the current density intercept at the ordinates points out the hydrogen evolution contribution to the overall current.

In order to determine the kind of nucleation mechanisms, the model developed by Scharifker and Hills [35] is used. In this model, the Instantaneous nucleation, which follows the equation 10 [35,36], corresponds to the immediate formation of all nuclei once the potential step is applied. While, the progressive nucleation, characterized by the equation 11 [35,36], describes the phenomenon of the permanent formation of the nuclei on the surface of the substrate and on the nuclei previously deposed.

$$\frac{i^2}{i_m^2} = \frac{1.9542}{\frac{t}{t_m}}\left(1 - \exp\left(-1.2564\left(\frac{t}{t_m}\right)\right)\right)^2 \quad (10)$$

$$\frac{i^2}{i_m^2} = \frac{1.2254}{\frac{t}{t_m}}\left(1 - \exp\left(-2.3367\left(\frac{t}{t_m}\right)^2\right)\right)^2 \quad (11)$$

where j_{max} and t_{max} are the coordinate of the maximum point in Figure 5.

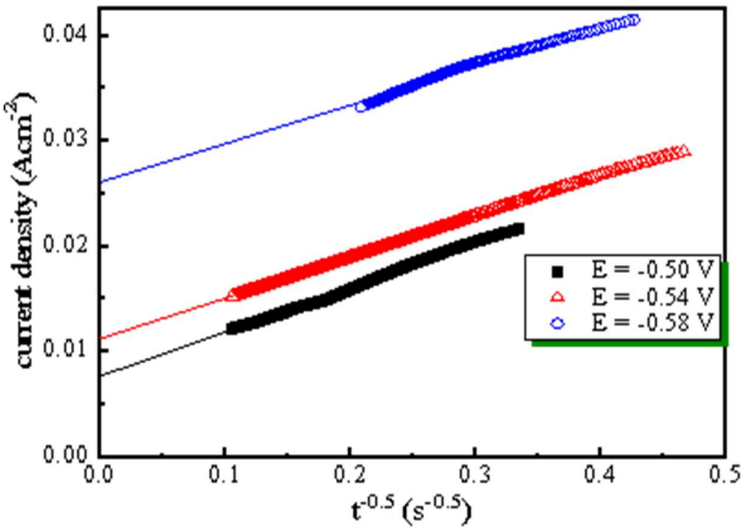

Fig. 6. Cottrell plots at different potentials in solution containing 0.14 M of $SnSO_4$ and 0.56 M of H_2SO_4

Figure 7 shows the theoretical (calculated from equations 10 and 11) and the experimental current transients plotted in the reduced current–time coordinates. According to this Figure, it is evident that the experimental curves show obvious deviations from the theoretical model indicating that the model of Scharifker and Hills is not able to give an acceptable interpretation of the nucleation process. Furthermore, as the applied potential shifts negatively, the deviation becomes more pronounced. Such behaviour is attributed to the parallel reaction of hydrogen evolution [37,38]. In order to get a depth insight into the contribution of the proton reaction current in the total current the Palomar–Pardavé model is used. In the transition curve, the variation of the total current density with time is given by [38]:

$$i(t) = (P_1 + P_4 t^{-\frac{1}{2}})x(1 - \exp\left[-P_2\left(t - \frac{1-\exp(-P_3 t)}{P_3}\right)\right]) \quad (12)$$

where

$$P_1 = Z_{PR} F K_{PR} (\frac{2CM}{\pi\rho})^{\frac{1}{2}} \quad (13)$$

$$P_2 = N_0 \pi D (\frac{8\pi C}{\rho})^{\frac{1}{2}} \quad (14)$$

$$P_3 = A \tag{15}$$

$$P_4 = 2FC\left(\frac{D}{\pi}\right)^{\frac{1}{2}} \tag{16}$$

where k_{PR} is the rate constant and $Z_{PR}F$ is the molar charge transferred during the proton reduction reaction. A is the nucleation rate. N_0 refers to the density of nucleation sites on the electrode surface. C is the bulk concentration of tin ion, M is the molar mass of Sn, ρ is the density of tin and D expresses the average value of the diffusion coefficient of tin ion. The non-linear fitting method based on Marquardt–Levenberg algorithm is used to fit the experimental current transients with equation 12. P_1, P_2, P_3 and P_4 were allowed to vary freely during the fitting operation.

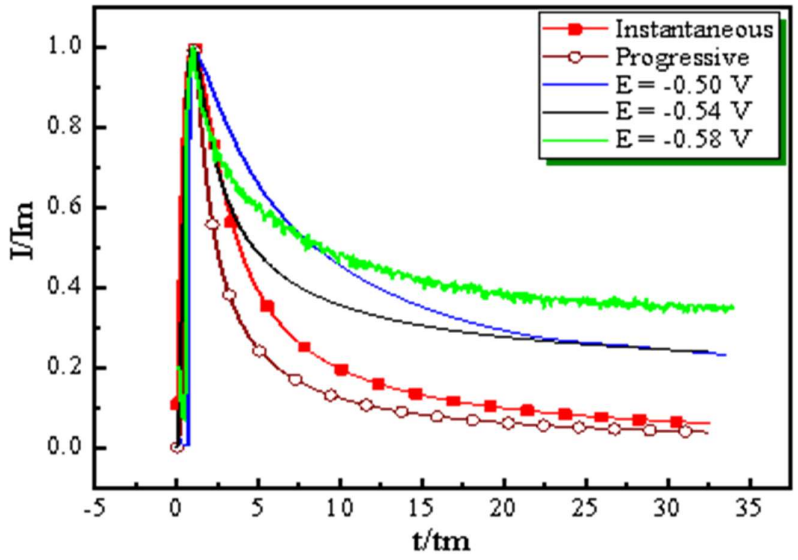

Fig. 7. Comparison of experimental and theoretical non-dimensional curves for nucleation model for tin electrodeposition on copper in 0.14 M $SnSO_4$ + 0.56 M H_2SO_4 at different potentials

Figure 8 shows the experimental transient curves obtained at different steps of the potential (-500, -540 and -580 mV), the corresponding fitting curves and the individual contributions of the tin and proton reduction to the overall experimental current densities. As can be seen, for each potential, the fitting curve describes closely the experimental current density.

The parameters P_1, P_2, P_3 and P_4 obtained from the fitting results are listed in Table 2. As can be noted, the increase in the cathodic overpotential is accompanied by an increase in the proton reaction rate constant k_{PR}, the density of nucleation sites N_0 and the nucleation rate

constant A respectively. $D = 6.78\times10^{-6}$ cm^2 s^{-1} is the average value of the stannous ion diffusion coefficient obtained from the values of P_1.

To get a detailed insight onto the tin electrodeposition process, the current coming from the proton reduction is separated from the whole current to obtain the current due to the tin reduction. The values corresponding to the falling part of the current originated from the tin reduction versus $t^{-1/2}$ yield a straight line (Fig. 9) confirming that this part obeys the Cottrell equation [36,39]. The stannous ion diffusion coefficients, at different potentials, calculated from the slopes of the curves in Figure 9 are presented in Table 3. The obtained values are close to those obtained above.

Table 2. Kinetic Parameters resulting from fitting according to the model described by Eq. 13 obtained at different stepped potentials.

Kinetic Parameters	E = -500 mV	E = -540 mV	E = -580 mV
P_1 (A cm^{-2} $s^{1/2}$)	0.008	0.0112	0.02456
P_2 (s^{-1})	1.088	1.39	1.813
P_3 (s^{-1})	1.06	1.09	1.853
P_4 (A cm^{-2})	0.041	0.038	0.04
A (s^{-1})	0.98578	1.77	1.853
N_0 (cm^{-2})	2.18×10^{6}	3.23×10^{6}	3.82×10^{6}
D (cm^2 s^{-1})	7.23×10^{-6}	6.24×10^{-6}	6.88×10^{-6}
K (mol cm^{-2} s^{-1})	1.09×10^{-6}	1.53×10^{-6}	3.35×10^{-6}

Table 3. The values of diffusion coefficients determined from Cottrell equation at different potentials

Potential	-0.500 V	-0.540 V	-0.580 V
D (cm^2s^{-1})	6.7×10^{-6}	6.5×10^{-6}	7.4×10^{-6}

The Scharifker and Hills models (Eq. 13 and 14) applied to the current densities of the tin ion reduction at different step potential is presented in Figure 10. The figure shows clearly the progressive nucleation characterizes the process of tin electrodeposition.

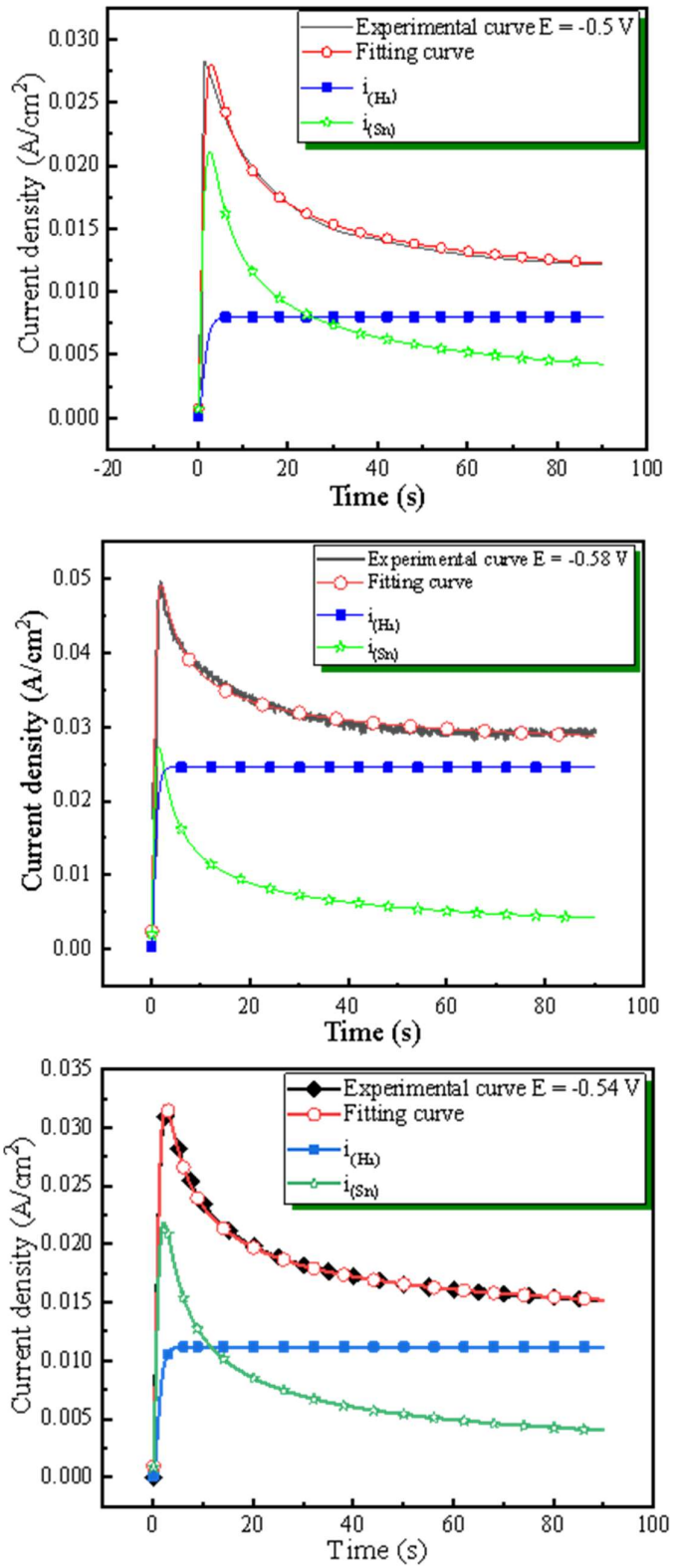

Fig. 8. Comparison between experimental transient, fitting of Eq. 13 current transient, $i_{(H2)}$ hydrogen evolution current and $i_{(Sn)}$ current due to the tin reduction at different potentials in solution containing 0.14 M of $SnSO_4$ and 0.56 M of H_2SO_4

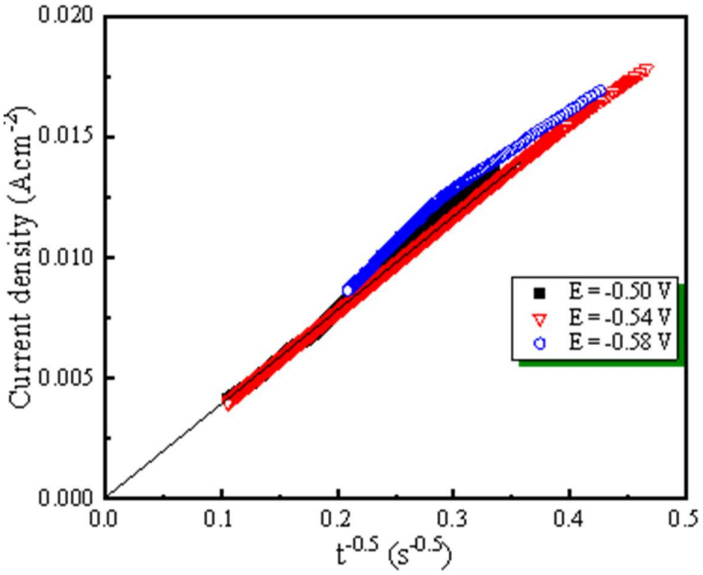

Fig. 9. Cottrell analysis of current transients due to the tin reduction at different potentials in solution containing 0.14 M of $SnSO_4$ and 0.56 M of H_2SO_4

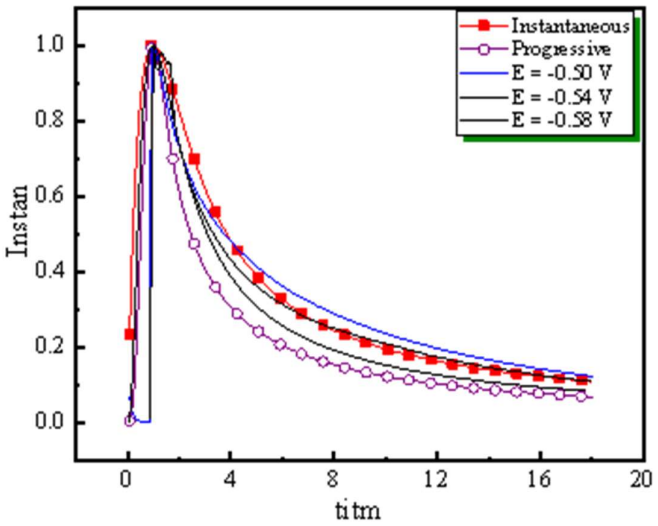

Fig. 10. Comparison of experimental and theoretical non-dimensional curves for nucleation model for current due to the tin reduction in 0.14 M $SnSO_4$+0.56 M H_2SO_4 at different potentials

Figure 11 displays the effect of the cathodic overpotential on the hydrogen evolution. It can also be seen, from this figure that, under our experimental conditions, the contribution of hydrogen evolution to the whole transition current begins at low overpotential and increases with increasing applied overpotential.

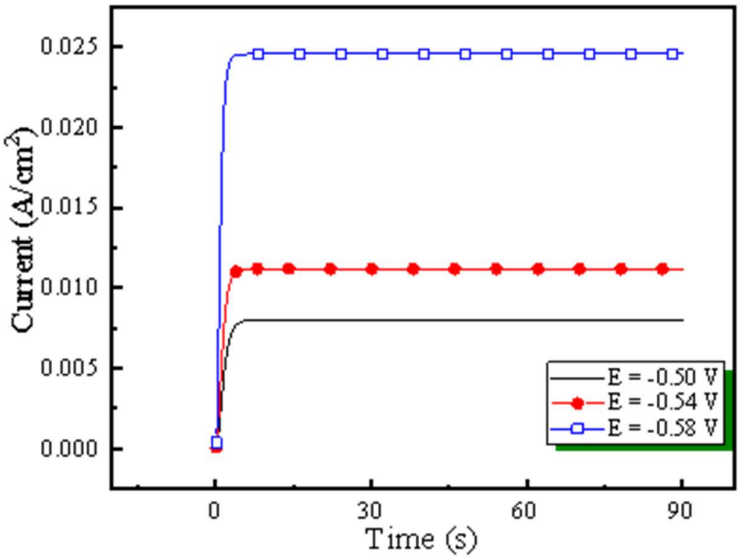

Fig. 11. The hydrogen evolution current at different potentials in solution containing 0.14 M of $SnSO_4$ and 0.56 M of H_2SO_4

4. CONCLUSION

Tin electrodeposition on copper from a solution composed of tin sulphate and sulphuric acid has been investigated. Electrochemical and surface characterization are used to provide a good understanding of the deposition process. Under our experimental conditions, the Sn^{2+}/Sn is an irreversible system. The morphology of the deposited tin is found to be influenced by the deposition current density. The obtained tin diffusion coefficient values are close. The current–time transients are found to match well with the Palomar-Pardavé model. This model reveals that hydrogen evolution should be taken into account because of the tin reduction occurs in parallel with the proton reduction even though at low overpotential. Chronoamperometric findings show that when the overpotential increases catholically, the reaction rate constant of the proton k_{PR}, the density of nucleation sites N^0 and the nucleation rate constant A also increase. Chronoamperogramms reveals that the tin nucleation, at the studied overpotential, conforms to an instantaneous nucleation mechanism.

REFERENCES

[1] W. J. Plumbridge, R. J. Matela, and A. Westwater, Structural Integrity and Reliability in Electronics Enhancing Performance in a Lead-Free Environment Kluwer Academic Publishers Dordrecht (2003).

[2] M. Schlesinger, and M. Paunovic, 5th Edition John Wiley & Sons, Inc., Hoboken, New Jersey 2010.

[3] R. M. MacIntosh, Modern Electroplating, 3rd ed., F. A. Lowenheim, Editor, Wiley, New York (1974).

[4] S. P. Zajkoska, A. Mulone, W. E. G. Hansal, U. Klemen, R. Mann, and W. Kautek, Coatings 8 (2018) 79.

[5] D. Aranzales, J. H. O. J. Wijenberg, and M. T. M. Koper, J. Electrochem. Soc. 166 (2019) D283.

[6] M. Schlesinger, and M. Paunovic, Modern Electroplating, Wiley, Hoboken (2010) 139.

[7] E. Rudnik, and G. Włoch, Appl. Surf. Sci. 265 (2013) 839.

[8] X. Wen, X. Pan, L. Wu, R. Li, D. Wang, J. Zhang, and P. Yang, Appl. Phys. A 123, 423 (2017). https://doi.org/10.1007/s00339-017-0960-z.

[9] S. Sengupta, A. Patra, A. Mitra, S. Jena, K. Das, S. Basu Majumder, and S. Das, Appl. Surf. Sci. 441 (2018) 965.

[10] D. T. Mackay, M. T. Janish, U. Sahaym, P. G. Kotula, K. L. Jungjohann, C. B. Carter, and M. G. Norton, J. Mater. Sci. 49 (2014) 1476.

[11] F. Wang, L. Chen, C. Deng, H. Ye, X. Jiang, and G. Yang, Electrochim. Acta 149 (2014) 330.

[12] A. Sharma, S. Bhattacharya, R. Sen, B. S. B. Reddy, H. -J. Fecht, K. Das, and S. Das, Mater. Charact. 68 (2012) 22.

[13] S. Bakkali, T. Jazouli, M. Cherkaoui, M. Ebntouhami, N. El Hajjaji, and E. Chassaing, Plat. Surf. Finish. 90 (2003) 46.

[14] C. T. J. Low and F. C. Walsh, J. Electroanal. Chem. 615 (2008) 91.

[15] N. M. Martyak and R. Seefeldt, Electrochim. Acta 49 (2004) 4303.

[16] M. García-Gabaldón, V. Pérez-Herranz, E. Sánchez, and S. Mestre, J. Membr. Sci. 323 (2008) 213.

[17] J. W. Wu, G. F. Zhai, Q. Chen, J. Q. Wang, and G. Ren, Appl. Surf. Sci. 254 (2008) 7227.

[18] F. X. Xiao, X-. N. Shen, F-. Z. Ren, and A. A. Volinsky, Int. J. Miner., Metall. Mater. 20 (2013) 472.

[19] F. X. Xia, X. -N. Shen, F. -Z. Ren, and A. A. Volinsky, Int. J. Miner., Metall. Mater. 20 (2013) 472.

[20] D. Li, J. Wu, T. Liu, J. Liu, Z. Yan, L. Zhen, and Y. Feng, Chem. Eng. J. 375 (2019) 122024.

[21] D. H. Won, C. H. Choi, J. Chung, M. W. Chung, E. -H. Kim, and S. I. Woo, ChemSusChem 8 (2015) 3092.

[22] Y. Zhang, X. Zhang, A. M. Bond, and J. Zhang, Phys. Chem. Chem. Phys. 20 (2018) 5936.

[23] V. S. K. Yadav, Y. Noh, H. Han, and W. B. Kim, Catal. Today 303 (2018) 276.

[24] S. Bakkali, M. Cherkaoui, A. Boutouil, M. R. Laamari, M. Ebn Touhami, M. Belfakir, and A. Zarrouk, Surf. Interfaces 19 (2020) 100480.

[25] J. Lei, and J-. G. Yang, J. Chem. Technol. Biotechnol. 92 (2016) 861.

[26] F. C. Walsh, and C. T. J. Low, Surf. Coat. Technol. 288 (2016) 79.

[27] A. J. Bard, and L. R. Faulkner, Electrochemical Methods, Fundamentals and Applications, Wiley & Sons, New York (1980).

[28] C. M. A. Brettand, and M. O. Brett, Electrochemistry principles, Methods and Applications. Oxford University Press 1994.

[29] D. Pletcher, R. Greff, R. Peat, L. M. Peter, and J. Robinson, Instrumental Methods in Electrochemistry, 1st Edition, Woo head Publishing Limited (2010).

[30] F. Chen, Q. Sun, W. Gao, J. Liu, C. Yan, and Q. Liu, J. Power Sources 280 (2015) 227.

[31] J. Gonzalez-Velasco, Electroanalysis 6 (1994) 711.

[32] S. Bakkali, R. Touir, M. Cherkaoui, and M. Ebn Touhami, Surf. Coat. Technol. 261 (2015) 337.

[33] A. Survila, Z. Mockus, S. Kanapeckaitė, and M. Samulevičienė, Electrochim. Acta 50 (2005) 2879.

[34] D. Grujicic, and B. Pesic, Electrochim. Acta 47 (2002) 2901.

[35] G. Oskam, J. G. Long, A. Natarajan, and P. C. Searson, J. Phys. D: Appl. Phys. 31(1998) 1927.

[36] M. R. Majidi, K. Asadpour-Zeynali, and B. Hafezi, Electrochim. Acta 54 (2009) 1119.

[37] J. Lei, and J. Yang, J. Chem. Technol. Biotechnol. 92 (2017) 861.

[38] M. Palomar-Pardavé, B. Scharifker, E. M. Arce, and M. Romero-Romo, Electrochim. Acta 50 (2005) 4736.

[39] D. Grujicic, and B. Pesic, Electrochim. Acta 50 (2005) 4426.